Missouri University of Science and Technology
Scholars' Mine

Chemistry Faculty Research & Creative Works | Chemistry

01 Jun 2016

A New Set of Potential Energy Surfaces for HCO: Influence of Renner-Teller Coupling on the Bound and Resonance Vibrational States

Steve Alexandre Ndengué

Richard Dawes
Missouri University of Science and Technology, dawesr@mst.edu

Hua Guo

Follow this and additional works at: https://scholarsmine.mst.edu/chem_facwork

 Part of the Chemistry Commons, and the Numerical Analysis and Scientific Computing Commons

Recommended Citation

S. A. Ndengué et al., "A New Set of Potential Energy Surfaces for HCO: Influence of Renner-Teller Coupling on the Bound and Resonance Vibrational States," *Journal of Chemical Physics*, vol. 144, no. 24, American Institute of Physics (AIP), Jun 2016.
The definitive version is available at https://doi.org/10.1063/1.4954374

This Article - Journal is brought to you for free and open access by Scholars' Mine. It has been accepted for inclusion in Chemistry Faculty Research & Creative Works by an authorized administrator of Scholars' Mine. This work is protected by U. S. Copyright Law. Unauthorized use including reproduction for redistribution requires the permission of the copyright holder. For more information, please contact scholarsmine@mst.edu.

A new set of potential energy surfaces for HCO: Influence of Renner-Teller coupling on the bound and resonance vibrational states

Steve Alexandre Ndengué,[1] Richard Dawes,[1,a)] and Hua Guo[2]
[1]*Department of Chemistry, Missouri University of Science and Technology, Rolla, Missouri 65409, USA*
[2]*Department of Chemistry and Chemical Biology, University of New Mexico, Albuquerque, New Mexico 87131, USA*

(Received 13 May 2016; accepted 1 June 2016; published online 22 June 2016)

It is commonly understood that the Renner-Teller effect can strongly influence the spectroscopy of molecules through coupling of electronic states. Here we investigate the vibrational bound states and low-lying resonances of the formyl radical treating the Renner-Teller coupled $\tilde{X}^2A'$ and $\tilde{A}^2A''$ states using the MultiConfiguration Time Dependent Hartree (MCTDH) method. The calculations were performed using the improved relaxation method for the bound states and a recently published extension to compute resonances. A new set of accurate global potential energy surfaces were computed at the explicitly correlated multireference configuration interaction (MRCI-F12) level and yielded remarkably close agreement with experiment in this application and thus enable future studies including photodissociation and collisional dynamics. The results show the necessity of including the large contribution from a Davidson correction in the electronic structure calculations in order to appreciate the relatively small effect of the Renner-Teller coupling on the states considered here. *Published by AIP Publishing.* [http://dx.doi.org/10.1063/1.4954374]

I. INTRODUCTION

The formyl radical (HCO) is an important intermediate for chemical mechanisms in hydrocarbon combustion[1,2] and atmospheric chemistry.[3] The H and CO constituents are also, respectively, the most abundant atom and second most abundant molecule in the interstellar medium (ISM). As such the description of the H–CO interaction is of particular interest in astrophysics and astrochemistry since the rovibrational state populations and state-to-state transfer rates following inelastic collisions of these constituents are very sensitive to the details of the interaction.

HCO and its isotopologue DCO have been extensively studied since the early 1960's both experimentally and theoretically. There are several aspects to its low-lying PESs that give rise to interesting and complex, yet somewhat tractable dynamics. Having only three nuclear degrees of freedom and 15 electrons makes it accessible to high-level electronic structure methods. The dissociation energy (D_0) to ground state H + CO fragments is 5083 ± 8 cm^{-1} according to the latest ATcT database[4] which has overlapping uncertainties with a recent measurement by Zhang of 5060 ± 20 cm^{-1}.[5] Given the light mass of the H-atom, there are only a few bound states (see Table III). However, due to an avoided crossing with an excited electronic state, there is a pronounced barrier in the entrance channel of the adiabatic ground state PES, of about 1140 cm^{-1}.[6,7] One consequence of the barrier is that it contributes to a considerable number of Feshbach resonance states. These have been used as a benchmark for several theoretical methods developed to compute resonances.[8–12] The equilibrium geometry on the ground $\tilde{X}^2A'$ electronic state is bent but becomes degenerate with the low-lying excited $\tilde{A}^2A''$ state (T_0 = 9294 cm^{-1}) at linear geometries, together forming a Π-state. The two states interact through the Renner-Teller (RT) coupling mechanism which is strongest near linearity. Since the equilibrium geometry is linear for the $\tilde{A}^2A''$ state, photodissociation via UV excitation from the ground state produces highly rotationally excited CO products.[13–15] Moreover, likely due to quantum interference effects induced by the topographies of the coupled PESs, oscillatory structure is imposed on the inverted product rotational state distribution envelope. The $\tilde{X}^2A'$–$\tilde{A}^2A''$ state degeneracy also occurs for linear geometries of HOC, but at higher energy, and a hanging minimum exists for a bent HOC structure on the ground electronic state. The energy of the HOC minimum is above the H + CO dissociation limit and even above the $\tilde{A}^2A''$ state minimum. Some harmonic frequencies for HOC have been published at the coupled-cluster level,[16] but in a more rigorous treatment, they would be seen only as localized resonance states and also subject to significant effects due to RT coupling. Scattering of H + CO involves some rather interesting dynamics and has been the subject of recent studies (so far neglecting the coupled $\tilde{A}^2A''$ state).[7] Since the CO bond energy is nearly 90 000 cm^{-1}, rather vigorous collisions will still ultimately only be rovibrationally inelastic, but not reactive. The barrier in the entrance channel produces threshold and resonance effects.

Experimentally, several techniques (fluorescence spectroscopy in a matrix or the gas phase, photodetachment spectroscopy, dispersed fluorescence spectroscopy, stimulated emission pumping, etc.) have been applied to characterize the bound and resonance states[13,17–23] as well as the product state distributions in various processes[14,15,24–26] (unimolecular dissociation, inelastic scattering, photodissociation) involving

a)dawesr@mst.edu

the radical. On the theory side, several investigations have been performed to complement and help interpret the experimental results.[27] In particular, more than 20 years ago, two groups produced sets of Potential Energy Surfaces (PESs) to describe the spectroscopy and dynamics of several processes of interest: unimolecular dissociation, photodissociation, inelastic scattering, etc. For convenience, we will refer in the following to the BBH[28,29] (Bowman, Bittman, and Harding) and WKS[30–32] (Werner, Keller, and Schinke) surfaces as the set of $\tilde{X}^2A'$–$\tilde{A}^2A''$ surfaces produced by the groups instead of only the ground state PESs that are usually referred to by those acronyms, although the BBH excited $\tilde{A}^2A''$ state was built by Goldfield, Gray and Harding.[29] The development of those PESs occurred during a period of intense experimental study and so those surfaces were refined on several occasions to better match emerging experimental data. The earlier BBH ground state ($\tilde{X}^2A'$) surface (which was actually a refined version of the *ab initio* PES) produced close agreement with earlier experimental results (see Refs. 20 and 28) but slightly worse with more recent results (see, for example, Table I). Experiments and calculations on the formyl radical have been shaping each other during the past decades and while qualitative agreement was reached via the earlier BBH surface, as commented by Werner *et al.*,[30] quantitative agreement is preferred to assure realistic interpretation of the dynamics. Recently, Song *et al.* made a 3D PES at the coupled-cluster level focusing on the long range interactions on the ground state.[6]

The electronic structure of the HCO molecule is surprisingly complex and difficulties with convergence were reported by Werner *et al.*[30] Our goal here is to construct an accurate enough set of PESs such that the details of the quantum mechanical treatment of the nuclear motion as well as the effects of Renner-Teller coupling can be meaningfully compared with experiment. Obtaining close enough agreement between theory and experiment will lend credibility to interpretations of the non-adiabatic dynamics of photodissociation and inelastic scattering. As we will discuss further in this article, the Renner-Teller effect perturbs various bound and resonance states to differing degrees but the improved agreement with experiment due to the RT effect is only appreciated once the PES is highly converged and a large Davidson correction is included.[33]

Section II describes our approach to construct a set of accurate coupled *ab initio* surfaces for HCO. The method of dynamically weighted state-averaged complete active space self-consistent field (DW-SA-CASSCF) calculations, overcomes previously noted convergence problems with this system[30] and yields a robust and consistent reference (with correct degeneracies etc.) for subsequent multireference configuration interaction (MRCI) calculations. However, some complications are noted due to internal contraction and Davidson corrections in the MRCI procedure. Following Sec. II, we will present the dynamical theory, i.e., the Hamiltonian, and the MCTDH algorithm for the quantum dynamics calculation and the improved relaxation method used to compute the bound and resonant states of the two coupled surfaces. Discussion, conclusions, and future directions follow.

TABLE I. Equilibrium parameters (valence coordinates, bohr, and degrees) and fundamental frequencies of the ground ($\tilde{X}^2A'$) and excited ($\tilde{A}^2A''$) states of the new HCO potential energy surfaces compared with previous results without consideration of the Renner-Teller coupling.

	This work	Exp.	WKS	BBH
$\tilde{X}^2A'$				
r_{CH} (a_0)	2.113	2.125[a]	2.110	2.116[b]
r_{CO} (a_0)	2.223	2.221[a]	2.233	2.259[b]
γ (deg)	124.34	124.95[a]	124.5	124.5[b]
ν_{HC} (cm^{-1})	2440.9	2434.5[c]	2437.2[d]	2448[b]
ν_{CO} (cm^{-1})	1862.4	1868.2[c]	1865.0[d]	1885[b]
ν_{bend} (cm^{-1})	1079.0	1080.8[c]	1079.3[d]	1104[b]
$\tilde{A}^2A''$				
r_{CH} (a_0)	2.014	2.01	2.007[e]	2.105[f]
r_{CO} (a_0)	2.234	2.23	2.248[e]	2.258[f]
γ (deg)	180.00	180.00	180.0	180.0[b]
ν_{HC} (cm^{-1})	3309.0	3319	3346[e]	3432[f]
ν_{CO} (cm^{-1})	1808.4	1812.2	1801[e]	1808[f]
ν_{bend} (cm^{-1})	804	805	808[e]	871[f]

[a]Reported by Brown *et al.* (Ref. 46).
[b]Reported by Bowman *et al.* (Ref. 28).
[c]Experimental values of Tobiason *et al.* (Ref. 23).
[d]Calculations reported by Keller *et al.* (Ref. 31).
[e]Reported by Loettgers *et al.* (Ref. 32).
[f]Results of Goldfield *et al.* (Ref. 29).

II. ELECTRONIC STRUCTURE AND PES

An *ab initio* based PES constructed at the MRCI level in 1995 by Werner *et al.* was described in two papers[30,31] and the first paper describes a rather complicated multistep procedure made necessary by issues with the electronic structure. Seeking primarily to fit the ground state, due to strong interactions they also included the two lowest excited $\tilde{X}^2A'$ and $\tilde{B}^2A'$ states in three state SA-CASSCF (equal weights) reference calculations, noting that despite testing a variety of combinations of active spaces and numbers of states, it was not possible to find an ansatz yielding good behavior globally (irregularities and lack of smoothness were encountered). They settled on a procedure that despite a reduced active space, and slight symmetry contamination, was deemed acceptably accurate.

Here, to promote convergence, all 18 doublet states (10 $^2A'$, 8 $^2A''$) formed by combining ground state H, C, and O-atoms were included in a generalized dynamic weighting (GDW-SA-CASSCF) procedure[34–39] using the full valence active space (thus the 18 doublet states are degenerate for three separate atoms). In contrast to the irregularities noted by Werner *et al.* the CASSCF convergence was robust and consistent throughout the coordinate ranges. In particular the correct degeneracy was obtained at linear geometries. However, the HCO system still does present two main difficulties for internally contracted *ic*MRCI calculations, those coming from (1) internal contraction and (2) the Davidson correction that was found necessary for quantitative accuracy (see Table III). The states of HCO except for linear geometries can be treated in C_s symmetry separated into

A' and A'' species. Due to internal contraction, when two *ic*MRCI states are computed for one symmetry species ($^2A'$ for the $\tilde{X}^2A'$ and $\tilde{B}^2A'$ states) and only one *ic*MRCI state for the other ($^2A''$ for the $\tilde{A}^2A''$ state), the two $^2A'$ states will be slightly lowered in energy, breaking the degeneracy with the $\tilde{A}^2A''$ state expected in the limit of linear geometries. For linear HCO, along the r_{CH} coordinate seam, the $^2A'$ state (expected to be degenerate) ranged from 106 cm^{-1} to 150 cm^{-1} below the $^2A''$ state, not only breaks the degeneracy, but the variation along the seam is such that a constant shift could not be applied to precisely correct the behavior. Adding additional reference symmetries to the calculation does not satisfactorily solve this issue. For HCO, the "brute force" solution of computing the three states on an equal footing without using C_s symmetry (only C_1) is effective (precise degeneracies were obtained) and somewhat affordable since there are only 15 electrons.

The second issue is that of the Davidson corrections.[33] There are several different Davidson corrections implemented in MOLPRO.[40] In our HCO calculations, the fixed reference Davidson correction was found to diverge wildly (corrections of more than 10 000 a.u. were common) in many locations where the CASSCF reference and MRCI data are sensible and well-behaved. Here the rotated reference correction based on the rotated reference energy (assigned to the variable `energd4` in MOLPRO) was found to be the most consistent, in terms of smooth sensible behavior. The magnitude of the correction was found to be significantly smaller than that of the relaxed reference correction using the non-rotated reference (the standard default correction assigned to the variable `energd`) at many geometries, especially for the excited states. In the entire data set (of nearly 8000 points), only five points were found to have divergent rotated Davidson corrections despite consistent behavior in the underlying MRCI data. They were simply identified as the locations of large positive disruptions ($\approx$10 000 cm^{-1}) in the interpolative fit, and thrown out. In addition, the rotated Davidson corrected energies for about 30 points caused slight interpenetration (reordering) of the states. For most of the points this was very slight (<10 cm^{-1}), but since the data set was fairly large and no one point is essential to constructing the fit, these points were also removed from the data set.

Benchmark calculations confirmed the importance of core-correlation[41] for the vibrational frequencies as well as for the dissociation energy and gaps to excited electronic states. Since the MRCI calculations were done without symmetry (to overcome the broken degeneracies that can be caused by internal contraction), and a large data set was anticipated in order to accurately represent three coupled electronic states, a medium sized basis was selected to manage cost. All-electron explicitly correlated (AE)-MRCI(Q_R)-F12 calculations with the CVQZ-F12 basis set could be closely matched with the triple-zeta CVTZ-F12 basis by applying a constant multiplicative scaling factor of 1.32 to the rotated Davidson correction. Thus the data for the PES were obtained at the (AE)-MRCI(Q_R^*)-F12/CVTZ-F12 level, where (Q_R^*) indicates scaling of the rotated Davidson correction. To make PESs for the three $\tilde{X}^2A'$, $\tilde{A}^2A''$, and $\tilde{B}^2A'$ and states simultaneously, keeping in mind that the topographies are significantly different for each state, it was decided to create a generously large data set in advance, rather than iteratively "grow" the PES as has been done for other systems.[42–45] Typically the automatically determined points depend on features of the surface and these are different for each state. Also, it is expected that a diabatization procedure between the derivative coupled $\tilde{X}^2A'$ and $\tilde{B}^2A'$ states will be performed in the future and that is best achieved with data for both states at each geometry using consistent orbitals. Data such as dipole and transition moments, as well as matrix elements of the electronic orbital angular momentum useful for describing RT coupling, were recorded as well. The behavior of the dipole moment for each state is shown in Figure 1 along the seam for linear geometries, illustrating the abrupt switch in character of the $\tilde{X}^2A'$ and $\tilde{B}^2A'$ states. In addition to a large set of 6000 points, globally distributed according to a Sobol sequence, additional batches totaling about 2000 points were generated adding to the density of coverage near linear geometries (HCO and HOC) as well as around local and global minima. Initially, the interpolating moving least squares (IMLS) fitting method was used to describe the coupled $\tilde{X}^2A'$ and $\tilde{B}^2A'$ adiabatic states. Once the five wildly divergent data points (mentioned above) were removed, consistent fits were obtained (shown in Figure 2). There, the r_{CO} distance was fixed at 1.18 Å and surface plots were made in Jacobi coordinates showing the shape of the PESs as a function of R_{CO-H} and theta. The degeneracy of the fits at linear geometries and behavior for small angles was already very good since the *ab initio* data itself is precisely degenerate as discussed above, the IMLS fitting is interpolative, and additional data was adding to these regions. To make it numerically exact, since the RT coupling

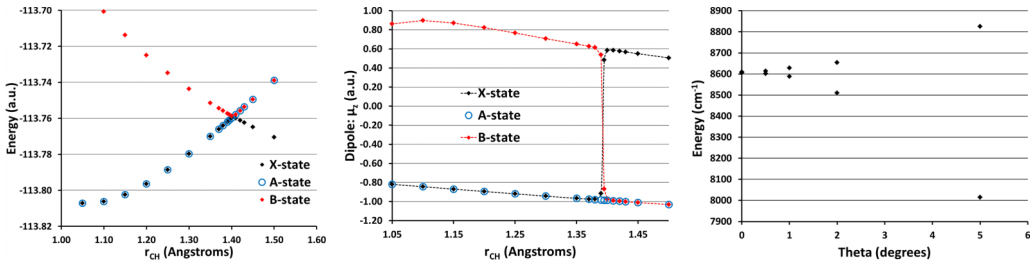

FIG. 1. (at left) Cut through the $\tilde{X}^2A'$, $\tilde{A}^2A''$, and $\tilde{B}^2A'$ states for linear geometries in valence coordinates. The energies are represented as a function of r_{CH} with the C–O bond distance fixed at $r_{CO} = 1.18$ Å and $\gamma = 180°$. (middle) Dipole moments (along the same cut as the energies at left) showing the abrupt switch in character between the $\tilde{X}^2A'$ and $\tilde{B}^2A'$ states. (at right) Energies of the Renner-Teller coupled $\tilde{X}^2A'$ and $\tilde{A}^2A''$ states are shown for small angles near the minimum of the degeneracy seam.

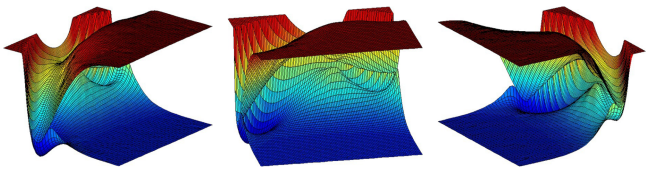

FIG. 2. 2D surface plots of the Renner-Teller coupled $\tilde{X}^2A'$ and $\tilde{A}^2A''$ states. The surfaces are represented in Jacobi coordinates as a function of R and γ with the C–O bond distance fixed at $r_{CO} = 2.23$ bohr. The seams of degeneracy are seen for linear geometries on the left (HCO) and right (HOC) sides of the plots.

is most relevant near linearity, a switching function was added (only turning on significantly in the last one degree before linearity), switching both PESs towards their average (and hence perfect degeneracy). Figure 1 plots the fitted $\tilde{X}^2A'$ and $\tilde{A}^2A''$ states for the last five degrees approaching linearity at the minimum point on the $\tilde{X}^2A'$–$\tilde{A}^2A''$ intersection seam.

We present results below for versions of the PESs with and without the Davidson correction and RT coupling effects. Here we briefly note, to summarize some of the features of the PESs, that results obtained using the best version of the PESs (including the rotated Davidson correction and the effects of RT coupling) are very close to experimental values and the best previous calculations. For example, using the ZPE we obtain for HCO (2795.3 cm^{-1} obtained in our calculations) and the ZPE of CO (1081.6 cm^{-1}) and the value of D_e evaluated at 15 bohrs on the PES (D_e = 6873 cm^{-1}) we obtain a value for the dissociation energy of D_0 = 5159 cm^{-1} which slightly exceeds the current ATcT database value of 5083 ± 8 cm^{-1}. The gap between the lowest vibrational levels on the $\tilde{X}^2A'$ and $\tilde{A}^2A''$ states is 9280 cm^{-1} which is remarkably close to the experimental value of T_0 = 9297 cm^{-1}.[46] The minimum of the $\tilde{A}^2A''$ state potential (relative to the minimum on the $\tilde{X}^2A'$ state) is at 8606 cm^{-1}. This puts the minimum of the degeneracy seam with the coupled $\tilde{A}^2A''$ state 1733 cm^{-1} above the asymptote. Due to the $\tilde{X}^2A'$– $\tilde{A}^2A''$ degeneracy, this value also represents the barrier to linearity, which is very close to the value to 1747 cm^{-1} reported by Song *et al.*[6] As will be discussed further below, having an accurate UV excitation energy in addition to realistic vibrational states on the $\tilde{A}^2A''$ state provides confidence in calculated photodissociation dynamics. As seen in Table I, the geometric parameters for both electronic states are very close to experiments and the best previous calculations. The gap from the minimum on the $\tilde{X}^2A'$ state to the Franck-Condon point above is 17 038 cm^{-1} although the excitation energy will be less due to ZPE effects. Finally, the barrier in the entrance channel is found to be 1140 cm^{-1} which is very close to the value of 1138 cm^{-1} obtained by Song *et al.*[6] in their careful study of the long range interaction region of this system.

III. QUANTUM NUCLEAR DYNAMICS

A. Hamiltonian

Vibrational calculations for triatomic molecules including the influence of the Renner-Teller effect have been reported by several authors (see Refs. 29, 32, and 47–52 to mention few). Jacobi coordinates are usually the coordinates of choice for these applications using either the so-called *R-embedding* or *r-embedding* where the z-axis is described by the H–CO or C–O vectors, respectively. Using the MCTDH algorithm, previous studies of nuclear dynamics and vibrational state calculations for coupled Renner-Teller electronic states made use of Valence coordinates[51,53,54] and also Jacobi coordinates.[48] Here we used Jacobi coordinates in the *r-embedding* representation to compute the bound vibrational states and resonances of the system. To construct the Hamiltonian, we follow the derivation given by Petrongolo[55] and used recently for a study of NH_2 by Zhou *et al.*,[47] for example. The total (electronic + nuclear) Hamiltonian representing the system is expressed in atomic units as

$$\hat{H} = -\frac{1}{2\mu_R}\frac{\partial^2}{\partial R^2} - \frac{1}{2\mu_r}\frac{\partial^2}{\partial r^2} + \hat{T}_{rot} + \hat{H}_{el}, \tag{1}$$

where the R and r coordinates represent the H–CO and C–O distances, respectively, with μ_R and μ_r their corresponding reduced masses. $\hat{T}_{rot}$ is given by

$$\hat{T}_{rot} = \hat{T}'_{rot} + \left(\frac{B+b}{\sin^2\gamma} - B\right)(\hat{L}_z^2 - 2\hat{J}_z\hat{L}_z), \tag{2}$$

with γ the angle between the two Jacobi vectors and the rotational constants B and b are

$$b = \frac{1}{2\mu_r r^2}, \qquad B = \frac{1}{2\mu_R R^2}. \tag{3}$$

The $\hat{T}'_{rot}$ operator has the usual form

$$\hat{T}'_{rot} = (B+b)\hat{j}^2 + B(\hat{J}^2 - 2\hat{J}_z^2 - \hat{J}_+\hat{j}_- - \hat{J}_-\hat{j}_+), \tag{4}$$

with

$$\hat{j}^2 = -\frac{1}{\sin\gamma}\frac{\partial}{\partial\gamma}\sin\gamma\frac{\partial}{\partial\gamma} + \frac{\hat{J}_z^2}{\sin^2\gamma} \tag{5}$$

and

$$\hat{j}_\pm = -cot\,\gamma\hat{J}_z \pm \frac{\partial}{\partial\gamma}, \tag{6}$$

$\hat{J}^2$, $\hat{J}_z$, and $\hat{J}_\pm$ are the squared total angular momentum, projection of J onto the BF z-axis, and the raising/lowering operators. $\hat{L}_z$ is the electronic angular momentum operator along the BF z-axis: the x and y components are usually neglected in the derivation of the equation,[29] since the coupling is only significant near linearity. For the $J = 0$ case, the Hamiltonian reduces to the simpler form

$$\hat{H} = -\frac{1}{2\mu_R}\frac{\partial^2}{\partial R^2} - \frac{1}{2\mu_r}\frac{\partial^2}{\partial r^2} + (B+b)\hat{j}^2 + \left(\frac{B+b}{\sin^2\gamma} - b\right)\hat{L}_z^2 + V(R,r,\gamma), \tag{7}$$

where $\hat{j}^2$ and $\hat{L}_z^2$ hold the same definitions as earlier and $\hat{L}_z^2$ is replaced by 1 in the calculation since $L_z = \pm 1$.

An alternative expression for the Hamiltonian may be obtained by replacing $\hat{J}_z$ by $\hat{N}_z$ in Equations (5) and (6). The resulting Hamiltonian is then

$$\hat{H} = -\frac{1}{2\mu_R}\frac{\partial^2}{\partial R^2} - \frac{1}{2\mu_r}\frac{\partial^2}{\partial r^2} + (B+b)\hat{j}^2 - b\hat{L}_z^2 + V(R,r,\gamma). \tag{8}$$

However, while for the Hamiltonian written according to Equation (7) an appropriate basis for the angular coordinate are Legendre polynomials (associated Legendre polynomials with $m = 0$), for the Hamiltonian of Equation (8), associated Legendre polynomials with $m = 1$ should be used since for $J = 0$, $\hat{N}_z^2 = \hat{L}_z^2 = 1$.

B. The MCTDH algorithm

The *Multiconfiguration Time Dependent Hartree*[56–58] (MCTDH) is an algorithm to solve the time dependent Schrödinger equation which can be considered as a sort of time-dependent version of the MultiConfigurational Self-Consistent Field (MCSCF) method applied to the nuclei. Within this method the wavefunction $\Psi(Q,t)$ of the system is written as a sum of products of *single-particle* functions (SPFs), forming a time-dependent orthonormal basis set.

The *ansatz* of the MCTDH wavefunction reads

$$\begin{aligned}\Psi(Q_1,\ldots,Q_f,t) &= \sum_{m_1}^{n_1}\cdots\sum_{m_p}^{n_p} A_{m_1,\ldots,m_p}(t)\Pi_{\kappa=1}^{f}\varphi_{m_\kappa}^{(\kappa)}(Q_\kappa,t),\\ &= \sum_{M} A_M\Phi_M, \end{aligned} \tag{9}$$

where f denotes the number of degrees of freedom of the system, the $A_M \equiv A_{m_1,\ldots,m_p}$ denote the MCTDH expansion coefficients and the configuration or Hartree products Φ_M are products of the SPFs defined in relation (9). The SPFs are finally represented by linear combinations of time-independent primitive basis functions

$$\varphi_{j_\kappa}^{(\kappa)}(Q_\kappa,t) = \sum_{l_1=1}^{N_{1,\kappa}}\cdots\sum_{l_1=1}^{N_{1,\kappa}} c_{j_\kappa l_1\ldots l_d}^{(\kappa)}(t)\chi_{l_1}^{(\kappa)}(Q_{1,\kappa})\cdots\chi_{l_d}^{(\kappa)}(Q_{d,\kappa}), \tag{10}$$

usually within a *discrete variable representation* (DVR),[59,60] here $\chi_{l_i}^{(\kappa)}(Q_i,\kappa)$, with the time dependent coefficients $c_{j_\kappa l_1\ldots l_d}$.

C. The improved relaxation and calculation of resonances

The improved relaxation method implemented in the Heidelberg MCTDH package is an MCSCF-like approach where the SPFs are optimized by relaxation (propagation in negative imaginary time)[61]and the coefficients vector (A-vector) are determined by the diagonalization of the Hamiltonian matrix evaluated in the set of SPFs. For bound states calculations, the block improved relaxation version[62] is usually used since it is more efficient when computing multiple eigenstates. The working equations of the improved relaxation have been presented before[58,63,64] and thus are not repeated here. We recently demonstrated (on the HCO system using the WKS PES)[8] how the improved relaxation method can be extended to compute resonances and also applied it to compute some resonances of ozone.[65] In short, the Hamiltonian is simply augmented with a Complex Absorbing Potential (CAP) and the relaxation no longer occurs in negative imaginary time but in the complex $(1,-1)/\sqrt{2}$ direction while the real part of the propagation is added to ensure that the wave-packet moves towards the CAP.

D. Details of numerical calculations

The calculation of bound and resonance vibrational states of HCO ($J = 0$) was performed as stated earlier in Jacobi coordinates using the *r-embedding*. Some calculations using the *R-embedding* were also done to check the consistency of the results. We obtain as expected that except for a tiny overall shift of the zero point energy for each of the embeddings, the vibrational energies were identical for the two calculations (the *R-embedding* Hamiltonian is obtained by swapping R and r in Equation (7) or (8)). The $\tilde{X}$ and $\tilde{A}$ states potential energy surfaces were refitted with the Potfit algorithm[66,67] implemented in the MCTDH package to obtain the sum-of-product form convenient for MCTDH calculations. The RMS error of the fit is small: less than 0.32 cm^{-1} and 0.16 cm^{-1} for the $\tilde{X}$ and $\tilde{A}$ states, respectively, for all point of energy less than 4 eV which belong to the range specified in Table II. In our tests, the Hamiltonians of Equations (7) and (8) were found to converge numerically to the same results. However, for vibrational states with amplitude near linearity (which is the case for most of the states computed for the $\tilde{A}$ electronic state), the singularity introduced by the $1/\sin^2\gamma$ term in Equation (7) makes that form of the Hamiltonian more difficult to converge. Equation (8) removes the singularity and is therefore more convenient for those states. Thus in our calculations, while the bound and resonance states on the $\tilde{X}$ state were obtained using Equation (7), Equation (8) was used to obtain results for the $\tilde{A}$ state (each using the appropriate angular basis).

As it was done in our previous paper on HCO resonances[8] the SPF basis was increased with increasing energy to better accommodate the nodal structure of higher vibrational states. The calculation of resonances proceeds in two steps at it was described before. First we perform a short time "bound" states calculation using a real artificial wall to identify states that are likely to be resonances. Then, for each of those states, individual CAP-added relaxations were performed and the positions and lifetimes were obtained for the resonances after a sufficiently long propagation time (usually several hundreds of fs). The form of the real repulsive wall, the CAP, and the optimization procedure that was used for the calculation was described before[8] and a similar procedure was used here. The results of our calculations are reported and discussed in Sec. IV.

TABLE II. Parameters of the primitive basis used for the vibrational bound and resonance states of HCO. Sine-DVR denotes Sine DVR. Leg-DVR are associated Legendre DVR with $m = 0$ or 1 for the Hamiltonians represented as Equations (7) and (8), respectively. The units are bohr and Radians.

	R	r	γ
Primitive basis	Sine-DVR	Sine-DVR	Leg-DVR
Number of points	196	128	128
Range	1.5–10.0	1.5–3.5	0-2π
Size of SPF basis	15–30	10–20	15–45

IV. RESULTS AND DISCUSSION

In Table III three sets of results for the vibrational bound states of HCO in the ground electronic state are reported illustrating the effects of the Davidson correction and RT coupling: without the Davidson correction (2nd column), with the Davidson correction (3rd column as described in Section II), and with the Davidson correction plus the Renner-Teller coupling (4th column). The values are compared with previous computations done on the WKS potential[31] (5th column) and experimental results[23] (last column). The last two lines show, respectively, the Mean Absolute Deviation (MAD) and Root Mean Square Error (RMSE) of the calculations with respect to experimental values. This table clearly shows the importance of the Davidson correction to the vibrational state calculations as the MAD and RMSE are reduced by an order of magnitude by its inclusion. The subsequent addition of the Renner-Teller coupling to the calculation for the ground electronic state improves only slightly the accuracy on average but more significantly the states with bending mode excitation (ν_2 mode). This behavior is expected since the equilibrium geometry on the ground state is bent and the wavefunction only explores towards linearity (where the RT coupling effect is significant) when there are multiple quanta in the bending mode.

The HCO($\tilde{A}^2A''$) is linear at equilibrium, and thus $J = 0, K = 0$ vibrational state calculations without the inclusion of the Renner-Teller coupling gives a progression of states with "even" bending quanta only, consistent with a linear molecule vibrational Hamiltonian. When the Renner-Teller coupling is included, due to its contribution of angular momentum, we instead observe the "odd" bending mode progression in the vibrational spectrum. (Consistent with the linear molecule Hamiltonian, these states are obtained in $J = 1, K = 1$ calculations without the RT terms.) In this study, for our calculations on the $\tilde{A}^2A''$ electronic state including the effects of RT-coupling, we focus on $J = 0, K = 0$ calculations, thus obtaining the "odd" progression which is compared with experiment in Table V. The calculations with RT-coupling

TABLE III. Comparison of calculated bound vibrational states of HCO($\tilde{X}^2A'$) with previous calculations[31] on the WKS surface and experiments,[23] exploring the effects of the Davidson correction and Renner-Teller coupling. The vibrational modes (ν_1, ν_2, and ν_3) in the first column are, respectively, the CO-stretch, bend, and CH-stretch.

(ν_1, ν_2, ν_3)	No Dav	Davidson	Dav + RT	WKS	Expt.
0,0,0	0	0	0	0	0
0,1,0	1106.5	1079.0	1081.4	1079.3	1080.8
0,0,1	1920.0	1862.4	1862.3	1865	1868.2
0,2,0	2167.5	2139.5	2144.7	2139	2142
1,0,0	2548.5	2440.9	2439.2	2437.2	2434.5
0,1,1	3021.2	2937.6	2939.8	2939	2942
0,3,0	3209.2	3178.2	3187.3	3177	3171
1,1,0	3642.7	3477.3	3477.8	3478	3476
0,0,2	3811.5	3701.5	3701.4	3706	3709
0,2,1	4085.8	3993.5	3998.5	3994	3997
0,4,0	4254.2	4188.9	4203.6	4191	4209
1,0,1	4478.3	4306.3	4304.4	4298	4302
1,2,0	4651.9	4479.4	4481.3	4475	4501
1,0,0	4788.3	4572.7	4570.2	4558	4570
0,1,2	4905.9	4773.9	4776.0	4775	4783
MAD	93.7	6.5	5.2	6.4	
RMSE	112.4	9.0	7.6	9.4	

TABLE IV. Comparison of vibrational states of HCO($\tilde{A}^2A''$) with the Davidson correction, but with and without the Renner-Teller contribution. The vibrational modes (ν_1, ν_2, and ν_3) in the first column are, respectively, the CO-stretch, bend, and CH-stretch. The vibrational states without Renner-Teller coupling are the origins of states computed for $J = 1, K = 1$ to permit comparison with Renner-Teller $J = 0, K = 0$ calculations (see text).

(ν_1, ν_2, ν_3)	Dav	Dav + RT	(ν_1, ν_2, ν_3)	Dav	Dav + RT
0,1,0	831.7	803.7	0,11,0	8 561.4	8 532.8
0,3,0	2447.2	2418.8	1,7,0	8 732.3	8 703.7
0,1,1	2636.7	2608.4	0,9,1	8 826.2	8 797.6
0,5,0	4008.7	3980.3	2,3,0	8 853.8	8 825.3
1,1,0	4117.0	4088.5	1,5,1	8 995.9	8 967.3
0,3,1	4238.4	4210.0	0,7,2	9 070.7	9 042.2
0,1,2	4421.1	4392.8	2,1,1	9 096.4	9 067.9
0,7,0	5551.8	5523.3	1,3,2	9 233.8	9 205.3
1,3,0	5695.5	5667.1	0,5,3	9 292.5	9 264.1
0,5,1	5786.9	5758.4	1,1,3	9 432.2	9 403.7
1,1,1	5907.5	5879.0	0,3,4	9 502.0	9 473.6
0,3,2	6009.2	5980.8	0,1,5	9 676.7	9 648.2
0,1,3	6190.5	6162.1	0,13,0	10 029.7	10 001.1
0,9,0	7069.0	7040.5	1,9,0	10 211.4	10 182.9
1,5,0	7226.5	7198.0	0,11,1	10 312.6	10 284.1
0,7,1	7319.0	7290.5	2,5,0	10 349.0	10 320.6
2,1,0	7319.8	7291.4	3,1,0	10 421.7	10 393.2
1,3,1	7475.2	7446.8	1,7,1	10 489.5	10 461.1
0,5,2	7548.3	7519.8	0,9,2	10 566.2	10 537.7
1,1,2	7679.4	7650.9	2,3,1	10 622.1	10 593.6
0,3,3	7764.4	7735.9	1,5,2	10 743.0	10 714.5
0,1,4	7943.5	7915.0	0,7,3	10 804.8	10 776.4

TABLE V. Comparison of $J = 0, K = 0$ vibrational states of HCO($\tilde{A}^2A''$) (in cm^{-1}) computed with inclusion of the Renner-Teller contribution with previous calculations[32] and experiments.[13] The values correspond to excitation from the (0,0,0) vibrational state of the $\tilde{X}^2A'$ electronic state. The vibrational modes (ν_1, ν_2 and ν_3) in the first column are, respectively, the CO-stretch, bend and CH-stretch. The number in parentheses are the differences from the experimental values of the 4th column.

(ν_1, ν_2, ν_3)	This work	Loettgers *et al.*	Expt.
0,1,0	10 089	10 289	
0,3,0	11 704 (43)	11 883 (222)	11 661
0,5,0	13 266 (44)	13 445 (223)	13 222
0,7,0	14 809 (50)	14 981 (222)	14 759
0,9,0	16 326 (52)	16 493 (219)	16 274
0,11,0	17 818 (57)	17 983 (222)	17 761
1,7,0	17 989 (54)	18 262 (327)	17 935
0,13,0	19 286 (59)	19 451 (224)	19 227
1,9,0	19 468 (63)	19 689 (384)	19 405
0,11,1	19 570 (56)	19 744 (230)	19 514
0,15,0	20 733 (65)	20 896 (228)	20 668
1,11,0	20 919 (67)	21 138 (286)	20 852
0,13,1	21 030 (64)	21 239 (273)	20 966
1,13,0	22 344 (73)	22 600 (329)	22 271
0,15,1	22 469 (72)	22 698 (301)	22 397

for $J = 0, K = 0$ only require a single electronic state as the RT-coupling term in Equation (7) or (8) for this case amounts to a potential-like term only (no mixing with the ground state). Thus the $J = 0, K = 0$ vibrational states on the $\tilde{A}^2A''$ electronic state are bound states with infinite lifetimes. The vibronic states and resonances for $K > 0$ (involving the two electronic states) are relevant to photodissociation processes and will be presented in a forthcoming publication. Here, for the $\tilde{A}^2A''$ state, in order to show the impact of the Renner-Teller effect on the vibrational states, we compare the vibrational band origins of $J = 1$ calculations without the RT-coupling terms (thus obtaining the odd bend progression), with those obtained with the RT-coupling terms for $J = 0, K = 0$. Table IV presents those results and highlights the effect of the Renner-Teller coupling on the bending mode progression.

Table V shows the vibrational states computed with $J = 0, K = 0$ with the RT contribution included. The results are compared with the previous calculations from Loettgers *et al.*[32] and with the experimental values of Loison *et al.*[13] The absolute excitation energies from the ground vibrational state of $\tilde{X}^2A'$ differ from the experimental values by at most 73 cm^{-1} and the spectrum is even better since all the values are systematically on average about 60 cm^{-1}

TABLE VI. Resonance positions and widths of HCO computed with MCTDH compared to previously reported calculations[a] and experiments.[b] The resonance positions are given relative to the ZPE of each surface. Note that the level notations follow those of Table III and differ from those of Ref. 8.

		Resonance positions (cm^{-1})				Resonance widths (cm^{-1})			
N	ν_1,ν_2,ν_3	No RT[c]	With RT[d]	WKS[a]	Experiments[b]	This work[c]	This work[d]	WKS[a]	Experiments[b]
1	0,3,1	5026.4	5035.3	5025.6	5032	2.60×10^{-7}	2.58×10^{-7}	4.00×10^{-8}	$<3.00 \times 10^{-1}$
2	0,5,0	5171.0	5194.2	5177.9	5204	4.18×10^{-7}	3.00×10^{-7}	2.38×10^{-6}	
3	1,1,1	5330.6	5330.4	5313.6	5324	1.11×10^{-6}	1.41×10^{-6}	1.01×10^{-3}	$<3.10 \times 10^{-1}$
4	1,3,0	5448.5	5451.6	5439.8		1.83×10^{-4}	2.06×10^{-4}	1.26×10^{-2}	
5	0,0,3	5517.2	5517.0	5522.7	5530	7.36×10^{-7}	5.88×10^{-7}	3.37×10^{-6}	$<2.30 \times 10^{-1}$
6	2,1,0	5562.2	5564.2	5560.3		1.45×10^{-3}	9.99×10^{-4}	5.65×10^{-2}	
7	0,2,2	5824.8	5829.6	5824.0	5834	6.86×10^{-5}	5.60×10^{-4}	7.61×10^{-4}	6.30×10^{-1}
8	0,4,1	6032.2	6046.2	6032.3	6038	2.92×10^{-3}	7.79×10^{-3}	7.34×10^{-1}	
9	0,6,0	6118.8	6157.3	6134.9		2.83×10^{-1}	1.31×10^{-1}	4.35×10^{-2}	
10	1,0,2	6167.0	6163.6	6150.6	6156	4.52×10^{0}	4.01×10^{0}	3.26×10^{0}	3.50×10^{0}
11	1,2,1	6317.3	6319.1	6386.9		1.13×10^{0}	1.20×10^{0}	2.31×10^{0}	
12	2,0,1	6480.1	6478.4	6477.5		2.91×10^{0}	3.37×10^{0}	1.07×10^{1}	
13	1,4,0	6531.9	6539.4	6531.2		2.73×10^{0}	2.56×10^{0}	1.59×10^{1}	
14	0,1,3	6586.9	6588.7	6587.4	6598	4.28×10^{-3}	4.15×10^{-3}	9.84×10^{-2}	4.60×10^{-1}
15	0,5,1	7008.9	7030.3	7004.2		8.30×10^{-1}	1.03×10^{0}	5.04×10^{0}	
16	0,7,0	7028.2	7097.0	7059.6		2.49×10^{-1}	6.06×10^{-1}	8.06×10^{-1}	
17	1,1,2	7170.8	7170.6	7159.1	7166	3.06×10^{0}	3.29×10^{0}	7.37×10^{0}	7.50×10^{0}
18	2,3,0	7223.7	7231.5	7178.1		2.60×10^{1}	2.87×10^{1}	6.75×10^{1}	
19	0,0,4	7309.0	7308.7	7315.0	7323	2.56×10^{-2}	2.27×10^{-2}	7.83×10^{-2}	2.40×10^{-1}
20	1,3,1	7328.3	7335.8	7336.4		6.40×10^{0}	8.33×10^{0}	1.72×10^{1}	
21	2,1,1	7436.2	7447.3	7439.1		1.43×10^{1}	9.22×10^{0}	2.24×10^{1}	
22	1,5,0	7474.9	7487.7	7492.3		5.28×10^{1}	5.84×10^{1}	5.79×10^{1}	
23	0,2,3	7633.0	7637.5	7631.6	7643	1.44×10^{-1}	1.46×10^{-1}	2.39×10^{-1}	2.80×10^{-1}
24	0,4,2	7853.2	7866.6	7848.5	7854	5.01×10^{-1}	6.52×10^{-1}	4.72×10^{0}	
25	1,0,3	7966.0	7963.4	7926.6		1.96×10^{0}	2.19×10^{0}	1.98×10^{1}	
26	0,6,1	7946.2	7976.9	7963.4	7957	1.04×10^{1}	2.14×10^{1}	1.00×10^{1}	8.80×10^{0}
27	1,2,2	8167.5	8168.4	8141.3	8156	1.37×10^{1}	1.34×10^{1}	2.31×10^{1}	1.80×10^{1}
28	1,4,1	8258.7	8273.6	8272.6		1.50×10^{1}	1.71×10^{1}	2.38×10^{1}	
29	0,1,4	8368.0	8364.6	8363.4	8390	7.39×10^{0}	1.07×10^{1}	1.01×10^{1}	1.70×10^{0}
30	0,3,3	8655.3	8663.3	8652.5	8666	2.07×10^{-1}	2.20×10^{-1}	7.28×10^{-1}	3.90×10^{-1}
31	0,7,1	8848.1	8893.1	8812.2		4.76×10^{1}	1.24×10^{2}	1.07×10^{1}	
32	1,1,3	8993.3	8993.0	8984.5	8988	9.33×10^{0}	9.40×10^{0}	1.71×10^{1}	1.65×10^{1}
33	0,0,5	9076.7	9076.3	9082.7	9092	4.08×10^{-2}	3.85×10^{-2}	5.44×10^{-2}	1.80×10^{-1}
34	1,3,2	9108.9	9113.6	9202.5		4.60×10^{1}	4.24×10^{1}	3.24×10^{1}	
35	0,2,4	9419.5	9423.5	9419.7	9431	9.60×10^{-1}	8.49×10^{-1}	6.03×10^{0}	1.20×10^{0}
36	0,4,3	9652.7	9665.2	9644.5	9663	9.49×10^{-1}	1.01×10^{0}	5.26×10^{0}	1.50×10^{0}
37	1,0,4	9765.1	9762.6	9749.8	9759	2.18×10^{0}	2.31×10^{0}	9.29×10^{0}	5.00×10^{0}
38	0,6,2	9759.5	9797.7	9772.8		8.66×10^{0}	8.66×10^{0}	6.18×10^{1}	
39	1,2,3	9954.5		9976.3	9992	2.31×10^{1}		3.59×10^{1}	4.50×10^{1}

[a]Calculations reported in Ref. 8 which compares with results of Refs. 9, 10, 31, and 68.
[b]Experimental results of Tobiason *et al.* (Ref. 23).
[c]Calculations done in this work without including the Renner-Teller coupling.
[d]Calculations done in this work with inclusion of the Renner-Teller contribution.

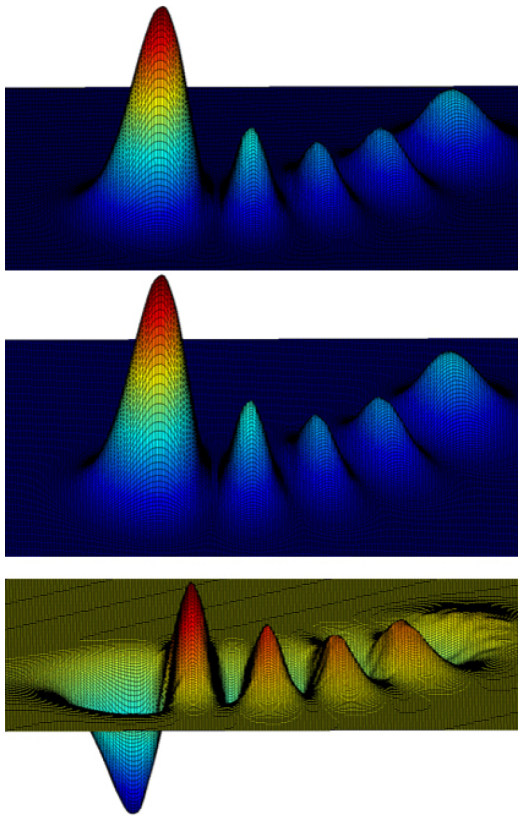

FIG. 3. Probability densities for the bend excited vibrational level (0,4,0) of the $\tilde{X}^2A'$ electronic state showing the effect of Renner-Teller coupling. The top and middle panels are without and with the RT-coupling, respectively. The bottom panel is the density difference which shows that the RT-coupling potential-like term, pushes density away from linearity (left side of plot). The energy is raised into better agreement with experiment see Table III.

too high. The states span an energy range of 12 500 cm^{-1} making the level of agreement quite remarkable. In the previous results by Loettgers *et al.*,[32] the errors are typically around 225 cm^{-1} for the $(0,v_2,0)$ progression and around 350 cm^{-1} for the $(1,v_2,0)$ progression. Thus the results obtained here with this new potential are substantially more accurate than those corresponding to the surface used for the Loettgers *et al.*[32] work. Reproducing both the absolute excitation energies as well as the spectrum of states places future studies of photodissociation dynamics on very firm ground.

We present in Table VI the ($J = 0$) resonances computed on the $\tilde{X}^2A'$ state. The calculations were done with and without the inclusion of the Renner-Teller effect. Results are compared with previous calculations (which compared well with other calculations)[8] done on the WKS surface and with experimental values from Tobiason *et al.*[23] The effect of the RT-coupling is most pronounced for states with many quanta in the bending mode. An effect of RT-coupling is that probability density is pushed away from the linear configuration, usually pushing up the energy level of that state. This is illustrated in Figure 3. Unfortunately experimental data are lacking for many of the most highly bend-excited states.

V. CONCLUSION

We present a new set of *ab initio* Potential Energy Surfaces for the Renner-Teller coupled ground $\tilde{X}^2A'$ and excited $\tilde{A}^2A''$ states of HCO. The electronic structure calculations are described for the coupled states and vibrational bound states are computed for both states. We also report resonance calculations beyond dissociation on the ground state surface with and without the consideration of the Renner-Teller effect in the 5000-10 000 cm^{-1} energy range above the ZPE. The calculations yield remarkably close agreement with experiments, including the absolute energies (above the $\tilde{X}^2A'$ state ZPE) of the spectrum of vibrational levels on the $\tilde{A}^2A''$ state. The results point to the importance of the Davidson correction and the need for more robust and better behaved corrections of this type. Consideration of the Renner-Teller effect is important to obtain quantitative agreement with experiment. Features of the ground $\tilde{X}^2A'$ are very similar to those recently reported by Song *et al.*[6] The electronic structure is well-enough converged to yield dynamical results of spectroscopic quality without iterative adjustment of empirical parameters.

A number of future directions are motivated by past experimental studies now that a quantitatively accurate PES for the coupled electronic states is in hand. Photodissociation and inelastic scattering calculations using the coupled surfaces to study the rovibrational product distribution are already underway and will be presented in the near future. Resonances calculations on the excited $\tilde{A}^2A''$ state using the MCTDH algorithm are also an interesting avenue as they require consideration of the coupled surface at relatively high energies: a problem that is challenging to treat with the improved relaxation method due to high state densities.

ACKNOWLEDGMENTS

This research was supported by the U.S. Department of Energy Office of Science, Office of Basic Energy Sciences [Award Nos. DE-SC0010616 to R.D. and DE-FG02-05ER15694 to H.G.]. S.A.N. thanks Hans-Dieter Meyer for discussions on the usage of the MCTDH package for the calculations reported in this work.

[1]J. Warnatz, in *Combustion Chemistry*, edited by W. C. Gardiner, Jr. (Springer, 1984), pp. 197–360.
[2]A. Gaydon, *The Spectroscopy of Flames* (Springer Science & Business Media, 2012).
[3]B. J. Finlayson-Pitts and J. N. Pitts, Jr., *Atmospheric Chemistry. Fundamentals and Experimental Techniques* (John Wiley and Sons, New York, NY, 1986).
[4]B. Ruscic, Active Thermochemical Tables (ATcT), values based on ver. 1.118 of the Thermochemical Network (2015); available at ATcT.anl.gov.
[5]J. Zhang, UC-Riverside, personal communication of unpublished results, 2015.
[6]L. Song, A. van der Avoird, and G. C. Groenenboom, J. Phys. Chem. A **117**, 7571 (2013).
[7]L. Song, N. Balakrishnan, A. van der Avoird, T. Karman, and G. C. Groenenboom, J. Chem. Phys. **142**, 204303 (2015).
[8]S. A. Ndengué, R. Dawes, F. Gatti, and H. D. Meyer, J. Phys. Chem. A **119**, 12043 (2015).
[9]J. C. Tremblay and T. Carrington, Jr., J. Chem. Phys. **122**, 244107 (2005).
[10]B. Poirier and T. Carrington, Jr., J. Chem. Phys. **116**, 1215 (2002).

[11]T. P. Grozdanov, V. A. Mandelshtam, and H. S. Taylor, J. Chem. Phys. **103**, 7990 (1995).
[12]D. Xie, R. Chen, and H. Guo, J. Chem. Phys. **112**, 5263 (2000).
[13]J. C. Loison, S. H. Kable, P. L. Houston, and I. Burak, J. Chem. Phys. **94**, 1796 (1991).
[14]S. H. Kable, J. C. Loison, P. L. Houston, and I. Burak, J. Chem. Phys. **92**, 6332 (1990).
[15]D. W. Neyer, S. H. Kable, J. C. Loison, P. L. Houston, I. Burak, and E. M. Goldfield, J. Chem. Phys. **97**, 9036 (1992).
[16]A. V. Marenich and J. E. Boggs, J. Phys. Chem. A **107**, 2343 (2003).
[17]D. W. Neyer and P. L. Houston, in *The Chemical Dynamic and Kinetics of Small Radicals*, edited by K. Liu and A. Wagner, Advanced Series in Physical Chemistry Vol. 6 (World Scientific, Singapore, 1994).
[18]D. E. Milligan and M. E. Jacox, J. Chem. Phys. **41**, 3032 (1964).
[19]R. N. Dixon, Trans. Faraday Soc. **564**, 3141 (1969).
[20]K. K. Murray, T. M. Miller, D. G. Leopold, and W. C. Lineberger, J. Chem. Phys. **84**, 2520 (1986).
[21]A. D. Sappey and D. R. Crosley, J. Chem. Phys. **93**, 7601 (1990).
[22]G. W. Adams, X. Zhao, and R. W. Field, J. Mol. Spectrosc. **160**, 11 (1993).
[23]J. D. Tobiason, J. R. Dunlop, and E. A. Rohlfing, J. Chem. Phys. **103**, 1448 (1995).
[24]D. W. Neyer, X. Luo, P. L. Houston, and I. Burak, J. Chem. Phys. **98**, 5095 (1993).
[25]D. W. Neyer, X. Luo, I. Burak, and P. L. Houston, J. Chem. Phys. **102**, 1645 (1995).
[26]C. Stöck, X. Li, H.-M. Keller, R. Schinke, and F. Temps, J. Chem. Phys. **106**, 5333 (1997).
[27]K. Tanaka and E. R. Davidson, J. Chem. Phys. **70**, 2904 (1979).
[28]J. M. Bowman, J. S. Bittman, and L. B. Harding, J. Chem. Phys. **85**, 911 (1986).
[29]E. M. Goldfield, S. K. Gray, and L. B. Harding, J. Chem. Phys. **99**, 5812 (1993).
[30]H. J. Werner, C. Bauer, P. Rosmus, H. M. Keller, M. Stumpf, and R. Schinke, J. Chem. Phys. **102**, 3593 (1995).
[31]H. M. Keller, H. Floethmann, A. J. Dobbyn, R. Schinke, H. J. Werner, C. Bauer, and P. Rosmus, J. Chem. Phys. **105**, 4983 (1996).
[32]A. Loettgers, A. Untch, H. M. Keller, R. Schinke, H. J. Werner, C. Bauer, and P. Rosmus, J. Chem. Phys. **106**, 3186 (1997).
[33]E. R. Davidson and D. W. Silver, Chem. Phys. Lett. **52**, 403 (1977).
[34]M. P. Deskevich, D. J. Nesbitt, and H.-J. Werner, J. Chem. Phys. **120**, 7281 (2004).
[35]R. Dawes, A. W. Jasper, C. Tao, C. Richmond, C. Mukarakate, S. H. Kable, and S. A. Reid, J. Phys. Chem. Lett. **1**, 641 (2010).
[36]A. Li, D. Xie, R. Dawes, A. W. Jasper, J. Ma, and H. Guo, J. Chem. Phys. **133**, 144306 (2010).
[37]R. Dawes, P. Lolur, J. Ma, and H. Guo, J. Chem. Phys. **135**, 081102 (2011).
[38]B. J. Barker, I. O. Antonov, J. M. Merritt, V. E. Bondybey, M. C. Heaven, and R. Dawes, J. Chem. Phys. **137**, 214313 (2012).
[39]A. W. Jasper and R. Dawes, J. Chem. Phys. **139**, 154313 (2013).
[40]H. J. Werner, P. J. Knowles, G. K. Knizia *et al.*, MOLPRO, version 2012.1, a package of *ab initio* programs, 2012, see http://www.molpro.net.
[41]D. Feller, K. A. Peterson, and D. A. Dixon, J. Chem. Phys. **129**, 204105 (2008).
[42]R. Dawes, X.-G. Wang, A. W. Jasper, and T. Carrington, Jr., J. Chem. Phys. **133**, 134304 (2010).
[43]M. Majumder, S. A. Ndengue, and R. Dawes, Mol. Phys. **114**, 1 (2015).
[44]R. Dawes, P. Lolur, A. Li, B. Jiang, and H. Guo, J. Chem. Phys. **139**, 201103 (2013).
[45]R. Dawes, X.-G. Wang, and T. Carrington, Jr., J. Phys. Chem. A **117**, 7612 (2013).
[46]J. M. Brown and D. A. Ramsay, Can. J. Phys. **53**, 2232 (1975).
[47]S. Zhou, Z. Li, D. Xie, S. Y. Lin, and H. Guo, J. Chem. Phys. **130**, 184307 (2009).
[48]S. Gómez-Carrasco and H. Köppel, Chem. Phys. **346**, 81 (2008).
[49]A. Li, H. Han, and D. Xie, J. Chem. Phys. **135**, 104304 (2011).
[50]H.-G. Yu, J. T. Muckerman, and T. J. Sears, J. Chem. Phys. **116**, 1435 (2002).
[51]Z. Zhang, H. Ma, and W. Bian, J. Chem. Phys. **135**, 154303 (2011).
[52]J.-P. Gu, G. Hirsch, R. Buenker, M. Brumm, G. Osmann, P. Bunker, and P. Jensen, J. Mol. Struct. **517**, 247 (2000).
[53]C. McCurdy, W. Isaacs, H.-D. Meyer, and T. Rescigno, Phys. Rev. A **67**, 042708 (2003).
[54]M. Eroms, M. Jungen, and H.-D. Meyer, J. Phys. Chem. A **114**, 9893 (2010).
[55]C. Petrongolo, J. Chem. Phys. **89**, 1297 (1988).
[56]H. D. Meyer, U. Manthe, and L. S. Cederbaum, Chem. Phys. Lett. **165**, 73 (1990).
[57]M. H. Beck, A. Jäckle, G. A. Worth, and H. D. Meyer, Phys. Rep. **324**, 1 (2000).
[58]*Multidimensional Quantum Dynamics: MCTDH Theory and Applications*, edited by H. D. Meyer, F. Gatti, and G. A. Worth (Wiley-VCH, Weinheim, 2009).
[59]J. Echave and D. C. Clary, Chem. Phys. Lett. **190**, 225 (1992).
[60]H. Wei and T. Carrington, J. Chem. Phys. **97**, 3029 (1992).
[61]R. Kosloff and H. Tal-Ezer, Chem. Phys. Lett. **127**, 223 (1986).
[62]L. J. Doriol, F. Gatti, C. Iung, and H.-D. Meyer, J. Chem. Phys. **129**, 224109 (2008).
[63]H.-D. Meyer and G. A. Worth, Theor. Chem. Acc. **109**, 251 (2003).
[64]H.-D. Meyer, F. Le Quéré, C. Léonard, and F. Gatti, Chem. Phys. **329**, 179 (2006).
[65]S. Ndengué, R. Dawes, X. G. Wang, T. Carrington, Jr., Z. Sun, and H. Guo, J. Chem. Phys. **144**, 074302 (2016).
[66]A. Jäckle and H. D. Meyer, J. Chem. Phys. **104**, 7974 (1996).
[67]A. Jäckle and H. D. Meyer, J. Chem. Phys. **109**, 3772 (1998).
[68]V. A. Mandelshtam and A. Neumaier, J. Theor. Comput. Chem. **1**, 1 (2002).